Research Article | Vol. 28, No. 3 / 3 February 2020 / Optics Express 3442
Optics EXPRESS

Phase interrogation SPR sensing based on white light polarized interference for wide dynamic detection range

YOUJUN ZENG,[1,6] XUELIANG WANG,[1,6] JIE ZHOU,[1] RUIBIAO MIYAN,[1] JUNLE QU,[1] HO-PUI HO,[2] KAIMING ZHOU,[3] BRUCE ZHI GAO,[4] AND YONGHONG SHAO[1,5]

[1]*College of Physics and Optoelectronics Engineering, Key Laboratory of Optoelectronic Devices and Systems of Ministry of Education and Guangdong Province, Shenzhen University, Shenzhen 518060, China*
[2]*Department of Biomedical Engineering, The Chinese University of Hong Kong, Shatin, Hong Kong*
[3]*Aston Institute of Photonic Technologies, Aston University, Birmingham, B4 7ET, United Kingdom*
[4]*Department of Bioengineering and COMSET, Clemson University, Clemson, SC 29634, USA*
[5]*shaoyh@szu.edu.cn*
[6]*These authors contributed equal to the article*

Abstract: A phase surface plasmon resonance (SPR) sensing technology based on white light polarized interference in common-path geometry is reported. A halogen lamp is used as the excitation source of the SPR sensor. The fixed optical path difference (OPD) between p- and s-polarized light is introduced by a birefringence crystal to produce sinusoidal spectral interference fringes. The SPR phase is accurately extracted from the interference fringes using a novel iterative parameter-scanning cross-correlation algorithm. The dynamic detection range is expanded by tracking the best SPR wavelength, which is identified using a window Fourier algorithm. The experimental results show that the sensitivity of this SPR system was 1.3×10^{-7} RIU, and the dynamic detection range was 0.029 RIU. This sensor, not only simple to implement and cost efficient, requires no modulators.

1. Introduction

Surface plasmon resonance (SPR) sensing has the advantages of including high sensitivity and label-free real-time high-throughput detection of biomolecular interactions. SPR has been widely used in environmental monitoring, food safety, medical diagnosis, genomics and proteomics research [1–3]. The SPR phenomenon produces minimal reflectivity (the SPR dip) because the incident p-polarized light resonantly couples with a surface plasma wave at a specific angle or wavelength. The position of the SPR dip is very sensitive to changes in the refractive index of the sample at the sensing surface.

To monitor the shift of the SPR dip, different types of SPR interrogation technologies have been developed, such as intensity interrogation, angular interrogation, spectral interrogation and phase interrogation [4–6]. Compared with other SPR technologies, the phase interrogation SPR technique has the highest sensitivity, reaching up to between 10^{-8} and 10^{-9} RIU. However, the phase interrogation SPR technique has a narrow dynamic detection range (typically 10^{-4} RIU), which means that the refractive index change may easily exceed the dynamic detection range [7]. Thus, development of SPR sensors is essential to expanding the dynamic detection range of the phase interrogation SPR technique.

To expand the dynamic detection range of phase interrogation SPR sensors, Huang *et al* proposed a phase interrogation SPR sensor that combined phase detection and angular interrogation. In their system, a liquid crystal modulator (LCM) modulates the excitation light from the laser diode, and a photodiode array simultaneously records the intensity of the reflected

#382242 https://doi.org/10.1364/OE.382242
Journal © 2020 Received 6 Nov 2019; accepted 3 Jan 2020; published 24 Jan 2020

Optics EXPRESS

modulation light at different angles. The sensitivity and dynamic detection range of the system are 2.2×10^{-7} RIU and 0.06 RIU, respectively [8]. Markowicz *et al* proposed a highly sensitive phase interrogation SPR sensing technology, in which a phase retarder and a photo-elastic modulator (PEM) simultaneously modulates the reflected laser, while the 2nd and 3rd harmonics of the modulated frequency are analyzed to extract the SPR phase. With this method, a dynamic detection range of 10^{-2} RIU and a sensitivity of 2.89×10^{-7} RIU has been achieved [9].

The combination of spectral interrogation with phase detection is the essential advancement for highly sensitive SPR sensing with a wide dynamic detection range [10–12]. Ho *et al* developed a phase interrogation SPR technology based on a white-light spectral interferometry method that uses the optical path structure of the Michelson interferometer. The phase difference between the p- and s-polarized light was extracted, which resulted in a sensitivity and dynamic detection range of 10^{-7} RIU and 10^{-2} RIU respectively [7]. In addition, Ng *et al* reported a differential spectral phase interrogation SPR scheme that offers a dynamic detection range of 10^{-2} RIU [13]. To reduce the two-path noise coming from the Michelson interferometer structure, Ho *et al* developed a polarized spectral interference-based SPR scheme that has a common-path geometry, in which a birefringent crystal introduces a phase difference between the p- and s-polarized light. Meanwhile an LCM modulates the incident to extract the SPR phase change. The dynamic detection range and sensitivity reached 3×10^{-2} RIU and 2×10^{-8} RIU respectively [14]. Our group developed a common-path phase interrogation SPR imaging scheme. By combining wavelength scanning by a liquid crystal tunable filter and modulation of the excitation light intensity using an LCM, the experimental dynamic detection range and sensitivity of the sensor were 0.0138 RIU and 2×10^{-7} RIU, respectively. Operating under an imaging mode, the system has high potential for high-throughput detection [15].

Demodulating the SPR phase requires at least one electronic modulator such as LCM or PEM, which increases the complexity and costs of the system significantly, not to mention the higher chance of more noise getting into the system. Here, we report a phase interrogation SPR sensor based on white light spectral polarized interference with no need of any modulator. A birefringent crystal is incorporated to perform the function of a traditional modulators through the introduction of an additional fixed phase delay between the p- and s-polarized components of the incident light. Simultaneously, a new iterative parameter-scanning cross-correlation (IPSCC) algorithm is proposed to more accurately extract the SPR phase as compared to the conventional cross-correlation algorithm.

2. Experiment

2.1. Setup

Figure 1 shows the optical setup of our SPR sensor. White light from a halogen lamp is coupled into a multimode optical fiber with 1mm core diameter through a lens group L1 and L2. Ultraviolet and near infrared regions of the white light source is removed with the use of a bandpass filter (BF). The light rays emerging from the coupling fiber is collimated by another lens L3 to excite SPR through the inverted prism having a refractive index of 1.515. A polarizer P1 is used to produce a 45° polarized light with the p-polarized light to realize the polarized light interference between the p- and s-polarized light, which travel along a common-path. A 10^5 nm optical path difference (OPD) between the p- and s- polarized light is introduced by a custom-made birefringence crystal (Newsandgy, Fuzhou, China) whose central wavelength is 650 nm. A prism, a sensing chip with gold film and a sample cell constitute a sensing module in which the SPR phase difference between the p- and s-polarized light is produced. The thickness of the sensing gold film is about 49 nm. The polarized interference between the p- and s-polarized light emerging from the sensing module occurs in the direction of the polarizer P2, perpendicular to P1. The output interference light is coupled into a multimode optical fiber by a lens L4 and then

Optics EXPRESS

recorded by a spectrometer (Firefly 4000, CNI Laser, China). The resolution of the spectrometer is 0.2 nm, and the detectable spectrum range is from 380 to 1100 nm.

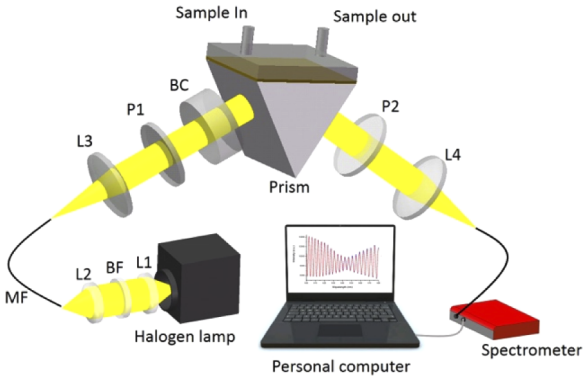

Fig. 1. Schematic of spectra-polarized interference-based SPR system: BF, bandpass filter; P1-2, polarizer; L1-4, lens; BC, birefringence crystal.

2.2. Algorithm

SPR introduces a dramatic shift in relative phase difference between the s- and p-polarization components at a specific wavelength. Meanwhile, the phase of the s-polarization component remains unaffected by SPR. The interference spectrum detected is determined by the OPD between the p- and s-polarized components. According to Fresnel formula [17,18], the interference spectrum can be expressed as:

$$I(\lambda) = I_0(\lambda)\{1 + V_{SPR}(\lambda)\cos[\phi_{OPD} + \phi_{SPR}(\lambda)]\} + I_{Noise} \quad (1)$$

in which $I_0(\lambda)$ is the light source spectrum, $V_{SPR}(\lambda)$ is the interference fringe contrast, ϕ_{OPD} is the additional phase difference between the p- and s-polarization components introduced by the birefringence crystal, and $\phi_{SPR}(\lambda) = |\phi_p - \phi_s|$ is the SPR phase.

The SPR phase shifts at different wavelengths due to changes in refractive indices are shown in Fig. 2(a). Generally it can be approximated that near resonance the SPR phase changes linearly with refractive index within a narrow range of refractive index (usually $\Delta n = 10^{-4}$ RIU) for a fixed excitation wavelength. We can expand the final dynamic detection range through cascading the adjacent linear ranges by selecting different excitation wavelengths according to the refractive index of the sample, as shown in Fig. 2(b). To better explain our SPR phase extraction method, we assume that the two groups of samples have respectively experienced a shift in refractive index from n_a to n_b and from n_i to n_{n+i} due to certain biomolecular binding events. The refractive index change of each group of samples is limited to the linear range of 10^{-4} RIU of a fixed excitation wavelength. In addition, the refractive index change of different groups of samples is large enough to go beyond the linear range. The interference spectra corresponding to n_a and n_b, n_i and n_{n+i} are respectively simulated and shown in Fig. 2(c) in different color plots. $n_0 n_1$ In the spectral region where SPR has taken place, the fringe contrast of the interference spectra will become low and becoming the weakest at the resonance wavelength. In our method propose herein, three main steps are involved for extracting the SPR phase:

1) Finding the resonance wavelength and differential operations on the interference spectra with respect to wavelength. First, the phase changes against wavelength are obtained by a windowed Fourier transform (WTF) algorithm [16]. Then, phase change rate at the excitation wavelength is calculated by performing differential operations on the phase

Optics EXPRESS

changes, as shown in Fig. 2(d). The wavelengths of λ_a and λ_b respectively represent the resonance wavelengths of the samples whose refractive index are n_a and n_b.

2) Intercepting the effective interference spectra from the whole interference spectra. We define the interference spectrum in $[\lambda_i - \frac{\Delta\lambda}{2}, \lambda_i + \frac{\Delta\lambda}{2}]$ as the effective interference spectrum at the resonance wavelength λ_i; in the wavelength range of $\Delta\lambda$, the SPR phase changes linearly with the refractive index of the samples. The effective interference spectrum (red curve) in $\left[\lambda_a - \frac{\Delta\lambda}{2}, \lambda_a + \frac{\Delta\lambda}{2}\right]$ for sample n_a is shown as a zoomed inset in Fig. 2(c).

3) Calculation of the SPR phase. The SPR phase is extracted by a new iterative parameter-scanning cross-correlation algorithm described in Section 3.1. If the refractive index of sample changes slightly from n_a to n_b, and the resonance wavelength is still in $\left[\lambda_a - \frac{\Delta\lambda}{2}, \lambda_a + \frac{\Delta\lambda}{2}\right]$, the SPR phase change can be extracted directly using the IPSCC algorithm. If the resonance wavelength jumps strictly out of $\left[\lambda_a - \frac{\Delta\lambda}{2}, \lambda_a + \frac{\Delta\lambda}{2}\right]$ because of the large step change of refractive index of sample, it is necessary to select a new effective spectrum range based on the new resonance wavelength, e.g., $\left[\lambda_i - \frac{\Delta\lambda}{2}, \lambda_i + \frac{\Delta\lambda}{2}\right]$, where we can still obtain the highly sensitive SPR phase change using our IPSCC algorithm. Finally, the total SPR phase change is calculated based on the following formula: $\Delta\emptyset_{Total} = \frac{\Delta\emptyset}{\Delta\lambda}(\lambda_i - \lambda_0) + \Delta\phi_i$; the first item is a low-precision measurement item based on the resonance wavelength change, and the second one is a high-precision phase measurement item.

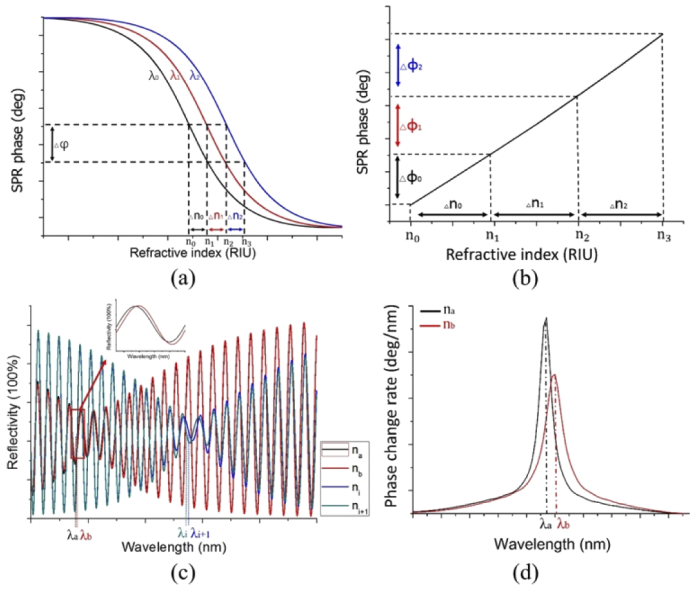

Fig. 2. (a) Phase change associated with SPR versus refractive index at different incident wavelengths; $\Delta n_0, \Delta n_1$ and Δn_2 represent the range of linear change of refractive index corresponding to λ_0, λ_1, and λ_2, respectively. (b) Linear phase change line with refractive index through cascading the multiple linear ranges of different wavelengths. (c) SPR interference spectra of two groups of samples (n_a and n_b, n_i and n_{i+1}) and amplified effective interference spectra extracted from the corresponding SPR interference spectra. (d) Phase change rate plotted against wavelength for two different refractive index values (n_a and n_b), which are calculated based on the corresponding SPR interference spectra of the samples.

Optics EXPRESS

3. Results and discussion

3.1. Iterative parameter-scanning cross-correlation algorithm

The cross-correlation algorithm is a common approach for extracting the phase information of signals. As shown in Equation (2), a cross-correlation coefficient R($-1 \leq R \leq 1$), in which x represents an ideal sinusoidal signal and y represents the detected signal, is a parameter that represents the degree of similarity of the two sets of signals. When |R|=1, the reference signal is completely correlated with the actual signal. The parameters including phase of the detected signal is exactly equal to ones of the reference signal. This kind of cross-correlation algorithm is usually used to extract the SPR phase in phase interrogation SPR technologies based on a constant period reference signal.

$$R = \frac{n\sum xy - \sum x \sum y}{\sqrt{n\sum x^2 - (\sum x)^2} \cdot \sqrt{n\sum y^2 - (\sum y)^2}} \tag{2}$$

However, the period of the actual signal in the spectral interference-based phase interrogation SPR technologies is not consistent with the period of the constant period reference signal due to resonance wavelength shift during the molecular interactions, which can lead to an increase in phase error and subsequently a degradation in the sensitivity of the SPR system. To solve the problem of phase errors introduced through the difference in periodicity, we propose a new IPSCC algorithm. The black plot in Fig. 3(a) shows how the calculated phase error varies with the period of the actual signal. From Fig. 3(a), it can be seen that as the period difference between the actual signal and the reference signal increases, so does the phase error. The red line in Fig. 3(a) shows the change of phase error versus the period of the actual signal. One can also see from this figure that phase error has been successfully suppressed using our new IPSCC algorithm.

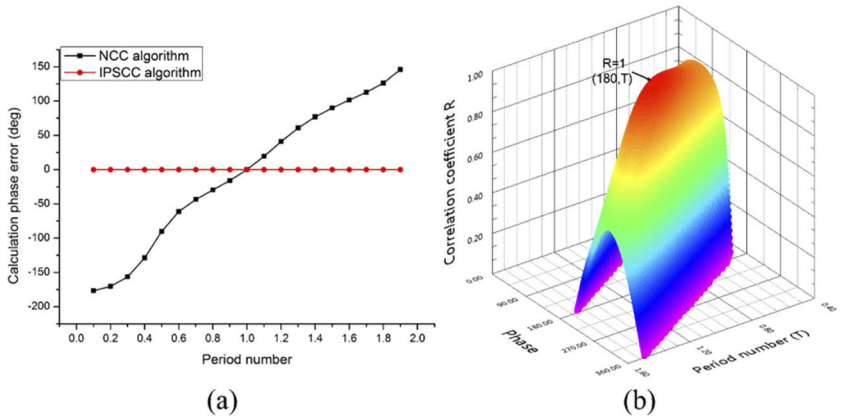

Fig. 3. Iterative parameter-scanning cross-correlation simulation. (a) Calculation phase errors simulated by normal cross-correlation (NCC) algorithm and IPSCC algorithm. (b) 3D plot of the change of cross-correlation coefficient with the phase and period number of reference signal. R = 1 when the phase is 180° and the period is T.

Specifically, our IPSCC algorithm mainly involves two steps. The first step is to scan the period of the reference signal, e.g., from 0.5T to 1.5T, in which T is a standard period in wavelength. The software generates a reference signal with a period T, such as $\cos\left(\frac{2\pi \cdot \Delta n \cdot d}{\lambda} + \phi\right)$, Δn is the refractive index difference between the p- and s-polarized light; d is the thickness of birefringence crystal; ϕ is the additional phase corresponding to that introduced by SPR phenomenon. Secondly,

Optics EXPRESS

to match the period and phase of the actual signals detected, a series of reference signals with the different periods and phase are produced based on the function: $\cos\left(\frac{2\pi\cdot\Delta n\cdot d}{\lambda_0 \pm \mathrm{M}\cdot\Delta\lambda} + \emptyset_0 \pm N\cdot\Delta\phi\right)$, $\mathrm{N, M} = 0, 1, 2, 3 \ldots..$ These reference signals are correlated with the actual signal in turn to generate a set of correlation coefficients among which the biggest correlation coefficient corresponds to the actual SPR phase. Taking the actual signal with a period of T and a SPR phase of 180 degree as an example, a three-dimensional plot of correlation coefficient change with the phase and period of the reference signal is shown in Fig. 3(b). R = 1 when the phase is 180 degree and the period is T.

3.2. Selection of additional OPD

The additional OPD between the p- and s-polarized light introduced by a birefringence crystal in our SPR system determines the density and structure of the interference fringes. To select the appropriate thickness of the birefringence crystal, the different additional OPD are simulated and discussed in this section. The SPR interference fringes under different additional OPD are shown in Fig. 4. The additional OPD in Fig. 4(a)-(d) is 5×10^4 nm, 7.5×10^4nm, 1×10^5 nm, and 5×10^5 nm, respectively. The simulated results indicate that the effective interference spectra near the resonance wavelength are not a sinusoidal signal until the additional OPD is about 7.5×10^4 nm. Fig. 4(b)-(d) show good sinusoidal fringes near the resonance wavelength, and the larger the additional OPD is, the denser the interference fringes become. Therefore, to produce good sinusoidal fringes, the birefringence crystal with an additional OPD of no less than 7.5×10^4 nm should be chosen in our SPR system.

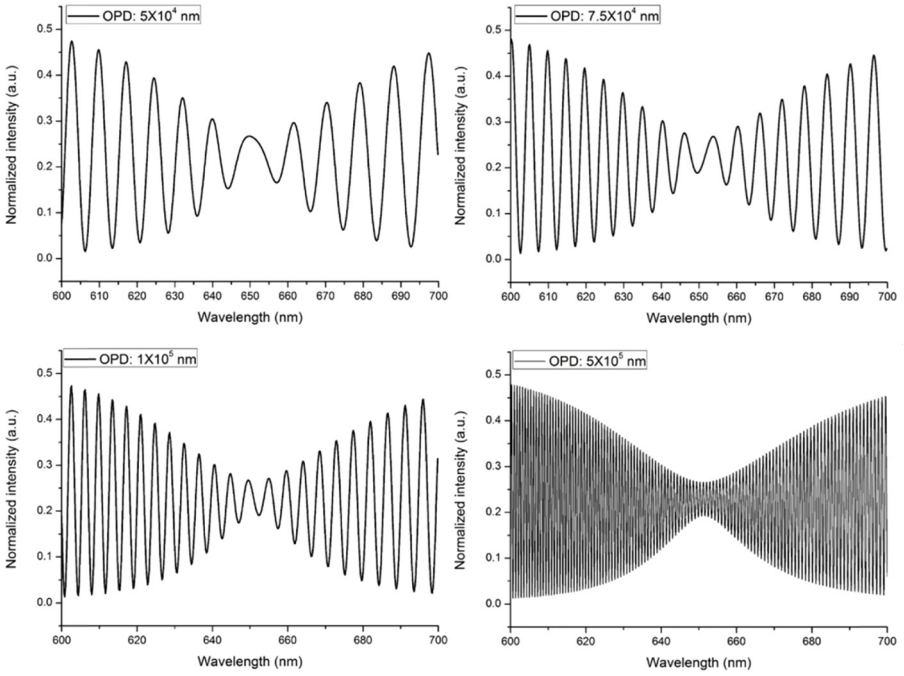

Fig. 4. SPR interference spectra obtained with different additional OPDs

To further analyze how the density of interference fringes affects the sensitivity of our SPR system, we theoretically simulate the change of the SPR phase with the change of refractive index under the different additional OPD of 7.5×10^4, 1×10^5, 1.25×10^5 and 5×10^5 nm respectively, as shown in Fig. 5. The corresponding sensitivities calculated are 1.34×10^{-7} RIU, 1.16×10^{-7}

Optics EXPRESS

RIU, 1.12×10^{-7} RIU, 9.09×10^{-8} RIU, respectively, under the root-mean-square (RMS) noise of 0.01 deg. Although a larger OPD is beneficial for achieving higher sensitivity, a detector with higher spectral resolution is required. In our experiment, we chose the birefringence crystal with an additional OPD of 10^5 nm because of the fact that our spectrometer with the spectral resolution of 0.2 nm.

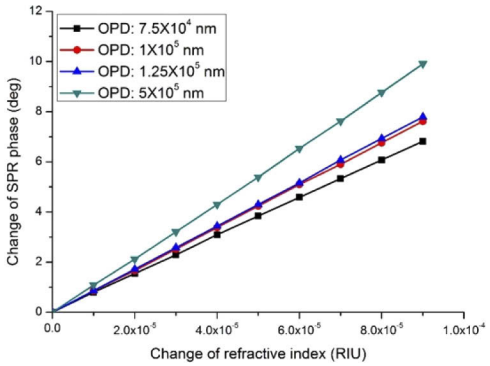

Fig. 5. Plots of phase versus refractive index under different additional OPDs.

3.3. Dynamic detection range and sensitivity

To measure the dynamic detection range of the system, we prepared sodium chloride solutions with concentrations ranging from 2% to 18% in increments of 2% by volume, corresponding to the refractive index range from 1.3367 to 1.3663 RIU. These solutions from low to high concentrations were consequently pumped into the sensing cell. The linear change of SPR phase with the sodium chloride concentrations ranging from 2% to 18% is shown in Fig. 6. The results indicate that the dynamic detection range of our SPR system reached 0.029 RIU.

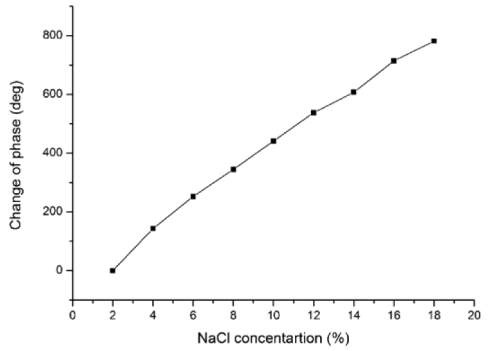

Fig. 6. Phase change with sodium chloride samples with concentration ranging from 0 to 18%.

Our SPR system's highest sensitivity corresponds to both the optimal excitation angle and wavelength for each refractive index of the sample. To simplify the structure of our SPR system, the incident angle is fixed, as will be at the cost of the sensitivity. To evaluate the sensitivity of the system in the whole dynamic detection range, we measure the system sensitivity at the different refractive index based on the different sodium chloride solutions with the concentrations of 2%, 3%, 4%, 6%, 8%, 10%, 12%, 14%, 16% and 18% through changing 0.1% of the concentration of each solution. For example, for 4% sodium chloride solution, the SPR phase change of the two

Optics EXPRESS

samples was monitored by injecting 3.9% and 4% sodium chloride solution one after another. The sensitivity of different samples is calculated using formula (3). The calculation results are shown in Fig. 7. The sensitivity reaches the highest of 1.3×10^{-7} RIU at 6% sodium chloride solution and the sensitivity in the whole dynamic detection range is in the order of 10^{-7} RIU.

$$\sigma_{RI} = \frac{\delta n}{\delta \varphi} \cdot \sigma_{SD} \tag{3}$$

in which σ_{RI} is SPR system sensitivity, δn is the change of refractive index of sample, $\delta \varphi$ is the SPR phase change, and σ_{SD} is the root mean square noise. In our sensitivity experiment, the root mean square noise was calculated 0.01 degree through monitoring the SPR phase of pure water for 30 minutes.

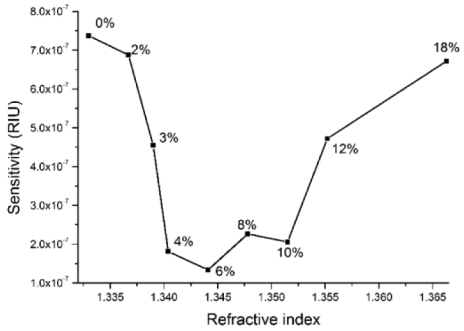

Fig. 7. Sensitivity calculated based on different samples.

4. Conclusions

We describe a white light polarization interference-based phase interrogation SPR sensing scheme that requires no modulator. Here, a birefringent crystal introduces a fixed large OPD between the p- and s-polarized light. The influence of the additional OPD on the interference spectra is analyzed through simulation. To improve the calculation accuracy of the SPR phase, a new IPSCC algorithm is described. The phase errors caused by the period difference of actual signals in the cross-correlation algorithm has been well suppressed. Our experiments revealed a system sensitivity and dynamic detection range of 1.3×10^{-7} RIU and 0.029 RIU respectively. The spectral resolution of the spectrometer limited the sensitivity of the SPR system in the experiments. If a spectrometer with a higher resolution of 0.02 nm, one could be used for the birefringence crystal with the larger OPD, the sensitivity of the SPR system could reach 10^{-8} RIU. The dynamic detection range of our SPR system was also limited by the halogen lamp's excitation wavelength range of 620 to 680 nm. The working spectral range of the birefringence crystal also affected the dynamic detection range. In theory, the larger the excitation wavelength range of the light source and the working spectral range of the birefringence crystal, the wider the dynamic detection range. It is possible to realize a spectral polarized interference-based SPR imaging using the wavelength-scanning technique previously reported by our group [15]. In conclusion, a highly practical spectral-phase interrogation SPR sensing scheme with high sensitivity and wide dynamic detection range is reported.

Optics EXPRESS

Funding

National Natural Science Foundation of China (61527827, 61775148); National Basic Research Program of China (973 Program) (2017YFB0403804); Guangdong Science and Technology Department (2017B020210006, 2018A030310544); Shenzhen Science and Technology Innovation Commission (JCYJ20180228162956597, JCYJ20180305124754860).

Disclosures

The authors declare no conflicts of interest.

References

1. B. Liedberg, I. Lundström, and E. Stenberg, "Principles of biosensing with an extended coupling matrix and surface plasmon resonance," Sens. Actuators, B **11**(1-3), 63–72 (1993).
2. L. Wu, J. Guo, X. Dai, Y. Xiang, and D. Fan, "Sensitivity Enhanced by MoS2–Graphene Hybrid Structure in Guided-Wave Surface Plasmon Resonance Biosensor," Plasmonics **13**(1), 1–7 (2018).
3. Y. Zeng, J. Zhou, X. Wang, X. Wang, and Y. Shao, "Wavelength-scanning surface plasmon resonance microscopy: A novel tool for real time sensing of cell-substrate interactions," Biosens. Bioelectron. **145**, 111717 (2019).
4. Y. Zeng, R. Hu, L. Wang, D. Gu, J. He, S. Y. Wu, H. P. Ho, X. Li, J. Qu, G. Bruce, and Y. Shao, "Recent advances in surface plasmon resonance imaging: detection speed, sensitivity, and portability," Nanophotonics **6**(5), 1017–1030 (2017).
5. D. Shi, W. Peng, and Y. Xinglong, "Phase-Sensitive Surface Plasmon Resonance Sensors: Recent Progress and Future Prospects," Sensors **17**(12), 2819–2833 (2017).
6. Y. Zeng, L. Wang, S. Y. Wu, J. He, J. Qu, X. Li, H. P. Ho, D. Gu, B. Z. Gao, and Y. Shao, "High-throughput imaging surface plasmon resonance biosensing based on an adaptive spectral-dip tracking scheme," Opt. Express **24**(25), 28303–28311 (2016).
7. S. P. Ng, C. M. L. Wu, S. Y. Wu, and H. P. Ho, "White-light spectral interferometry for surface plasmon resonance sensing applications," Opt. Express **19**(5), 4521–4527 (2011).
8. Y. Huang, H. P. Ho, S. Y. Wu, S. K. Kong, W. W. Wong, and P. Shum, "Phase sensitive SPR sensor for wide dynamic range detection," Opt. Express **36**(20), 4092–4093 (2011).
9. P. P. Markowicz, W. C. Law, A. Baev, P. N. Prasad, and A. V. Kabashin, "Phase-sensitive time-modulated surface plasmon resonance polarimetry for wide dynamic range biosensing," Opt. Express **15**(4), 1745–1754 (2007).
10. Y. Huang, H. P. Ho, S. Y. Wu, and S. K. Kong, "Detecting Phase Shifts in Surface Plasmon Resonance: A Review," Adv. Opt. Technol. **2012**, 1–12 (2012).
11. W. Yuan, H. P. Ho, C. L. Wong, S. K. Kong, and C. Lin, "Surface plasmon resonance biosensor incorporated in a Michelson interferometer with enhanced sensitivity," IEEE Sens. J. **7**(1), 70–73 (2007).
12. P. Hlubina, D. Ciprian, and J. Lunacek, "Spectral interferometric technique to measure the ellipsometric phase of a thin-film structure," Opt. Lett. **34**(17), 2661–2663 (2009).
13. S. P. Ng, C. M. L. Wu, S. Y. Wu, H. P. Ho, and S. K. Kong, "Differential spectral phase interferometry for wide dynamic range surface plasmon resonance biosensing," Biosens. Bioelectron. **26**(4), 1593–1598 (2010).
14. S. P. Ng, F. C. Loo, S. Y. Wu, S. K. Kong, C. M. L. Wu, and H. P. Ho, "Common-path spectral interferometry with temporal carrier for highly sensitive surface plasmon resonance sensing," Opt. Express **21**(17), 20268–20273 (2013).
15. Y. Shao, Y. Li, D. Gu, K. Zhang, J. Qu, J. He, M. G. Somekh, and H. Niu, "Wavelength-multiplexing phase-sensitive surface plasmon imaging sensor," Opt. Lett. **38**(9), 1370–1372 (2013).
16. S. P. Ng, S. Y. Wu, H. P. Ho, and C. M. L. Wu, "A white-light interferometric surface plasmon resonance sensor with wide dynamic range and phase-sensitive response," *IEEE International Conference on Electron Devices and Solid-State Circuits*, December 2008, HKSAR.
17. P. Hlubina, J. Luňáček, D. Ciprian, and R. Chebus, "Windowed Fourier transform applied in the wavelength domain to process the spectral interference signals," Opt. Commun. **281**(9), 2349–2354 (2008).
18. L. Li, C. Cheng, D. Han, Q. Sun, and G. Shi, "Phase Retrieval from Multiple-Window Short-Time Fourier Measurements," IEEE. Signal. Proc. Lett. **99**, 1 (2016).